PHYSICAL REVIEW B **87**, 104107 (2013)

Stability maps to predict anomalous ductility in B2 materials

Ruoshi Sun[1,2] and D. D. Johnson[1,3,4,*]

[1]*Materials Science and Engineering, University of Illinois at Urbana-Champaign, 1304 West Green Street, Urbana, Illinois 61801, USA*

[2]*Materials Science and Engineering, Massachusetts Institute of Technology, 77 Massachusetts Avenue, Cambridge, Massachusetts 02139, USA*

[3]*The Ames Laboratory, US Department of Energy, 311 TASF, Iowa State University, Ames, Iowa 50011-3020, USA*

[4]*Materials Science and Engineering, Iowa State University, Ames, Iowa 50011-2300, USA*

(Received 15 January 2013; revised manuscript received 5 March 2013; published 19 March 2013)

While most B2 materials are brittle, a new class of B2 (rare-earth) intermetallic compounds is observed to have large ductility. We analytically derive a *necessary condition* for ductility (dislocation motion) involving $\langle 111\rangle$ versus $\langle 001\rangle$ slip and the relative stability of various planar defects that must form. We present a *sufficient condition* for antiphase boundary bistability on $\{1\bar{1}0\}$ and $\{11\bar{2}\}$ planes that allows multiple slip systems. From these energy-based criteria, we construct two stability maps for B2 ductility that use only dimensionless ratios of elastic constants and defect energies, calculated via density functional theory. These two conditions fully explain and predict enhanced ductility (or lack thereof) for B2 systems. In the 23 systems studied, the ductility of YAg, ScAg, ScAu, and ScPd, ductile-to-brittle crossover for other rare-earth B2 compounds, and brittleness of all classic B2 alloys and ionic compounds are correctly predicted.

DOI: 10.1103/PhysRevB.87.104107 PACS number(s): 62.20.fk, 61.72.Nn, 81.05.Bx, 71.20.−b

I. INTRODUCTION

In 2003, Gschneidner *et al*. discovered a family of ductile rare-earth/transition-metal (RM) intermetallic compounds with the body-centered-cubic-based B2 (or CsCl) crystal structure.[1] The current list of known ductile B2 compounds can be found in Ref. 2. In contrast to the brittleness of classic B2 alloys, the ductility of YAg is comparable to face-centered-cubic Al, and YCu is half that of YAg. As line compounds are usually brittle,[3] the reason for anomalous ductility in RM compounds remains open. Moreover, some RM compounds, such as $(Tb_{0.88}Dy_{0.12})Zn$ (Ref. 4) and YMg,[5] are brittle. Hence, the questions: Why are they different? Can anomalous ductility be predicted on a system-dependent basis?

Much work has been done in determining the dominant slip systems of the B2 alloys. As discussed in the review articles by Yamaguchi and Umakoshi[6] and Baker,[7] $\langle 111\rangle$ and $\langle 001\rangle$ are the two main observed slip directions for dislocation motion in B2 materials (Fig. 1). Yet no previous theories have attempted to predict B2 ductility because all the known alloys and ionic compounds are brittle. For example, polycrystalline NiAl has only a 2% elongation upon fracture.[3] Baker concluded that limited ductility is associated with $\langle 001\rangle$ slip, and brittleness with $\langle 111\rangle$ slip.[7] While off-stoichiometric B2 alloys exhibit improved ductility, yield strength is sacrificed, which is not useful for practical purposes.[3] In contrast to B2 alloys, this new class of RM compounds has an exact stoichiometry, and the compounds are nearly elastically isotropic.[1]

Following the discovery of the RM compounds, there have been several experimental[4,8,9] and theoretical[2,10–12] studies. Morris *et al*. have hypothesized that the enhanced ductility in the Y-based compounds is due to the competing structural stability of B33 and B27 phases, obtained by introducing a periodic array of $\frac{a}{2}\langle 001\rangle\{1\bar{1}0\}$ superintrinsic stacking faults (SISFs) to the B2 lattice.[12] However, the fact that not all the RM-B2 compounds are ductile highlights the complications with classification of the slip modes and the prediction of their ductility. More recently, Gschneidner *et al*. established a correlation between the absence of *d* electrons and measured ductility.[2] However, a direct explanation from the perspective of ductility involving dislocation motion and defect energetics is lacking. Such a theory permits prediction, as well as correlations to specific electronic features, to be made, while relating observed ductility measures to features in the electronic structure is fruitful but not a theory.

To address the atypical ductility possessed by some RM compounds and the unresolved issue of predicting $\langle 111\rangle$ versus $\langle 001\rangle$ slip, we provide a quantitative explanation from mesoscale dislocation mechanics using energy-based stability criteria, whose parameters can be calculated from density functional theory (DFT). In short, we present a predictive theory for ductility in ideal B2 compounds. From stability criteria derived for the B2 structure, we provide a *necessary* and *sufficient* condition for increased ductility in B2 systems, which are displayed in terms of predictive dimensionless maps. We apply these maps to three types of B2 materials: (1) Y-based and Sc-based compounds (YAg, YCu, YIn, YRh, YMg, YZn, ScAg, ScAu, ScCu, ScPd, ScPt, ScRh, and ScRu), (2) classic alloys (NiAl, FeAl, AuCd, AuZn, CuZn, and AgMg), and (3) ionic compounds (CsCl, CsI, TlBr, and TlCl). Any proposed B2 compound can be added to the map to predict its relative ductility. The possibilities can be narrowed using only the Zener anisotropy ratio.

II. BACKGROUND

For dislocation-mediated deformation, both elastic anisotropy and planar defect energies (e.g., antiphase boundaries $\gamma_{\mathrm{APB}}^{hkl}$ or stacking faults $\gamma_{\mathrm{SF}}^{hkl}$) in the competing Miller-indexed (hkl) slip planes are relevant. Clearly, the more elastically isotropic a system, the easier for dislocation movement to other slip planes under shear. As noted, the new ductile B2 systems are nearly elastically isotropic,[1] with Zener anisotropy ratio A close to 1, where

$$A = \frac{2c_{44}}{c_{11} - c_{12}}. \tag{1}$$

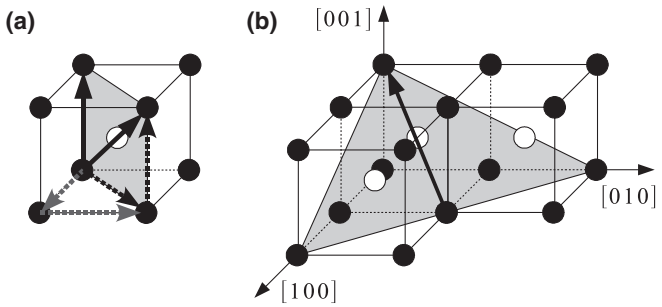

FIG. 1. For B2 systems, the (a) [001] and [111] slip in the $(1\bar{1}0)$ plane and (b) $[\bar{1}\bar{1}1]$ slip in the $(11\bar{2})$ plane. (a) Perfect ⟨111⟩ superdislocation can dissociate [Eq. (7a)] into perfect ⟨110⟩ and ⟨001⟩ dislocations (dashed lines), with possible dissociation of ⟨110⟩ into ⟨100⟩ and ⟨010⟩ (grey dashed lines).

Here, the c_{ij}'s are the cubic elastic constants, and, in particular, c_{44} is the shear modulus. For a B2 lattice constant of a, the product of $c_{44}a$ has units of γ (in mJ/m^2). For an energy-based criterion for ductility under shear, dimensionless ratios are relevant, reflecting relative energies; two ratios associated with the energetics of slip directions and defect formation, making the simple maps, are

$$C = \gamma_{\mathrm{APB}}^{1\bar{1}0}/c_{44}a, \tag{2}$$

$$\delta = \gamma_{\mathrm{SF}}^{1\bar{1}0}/\gamma_{\mathrm{APB}}^{1\bar{1}0}. \tag{3}$$

These quantities can be obtained via DFT calculations.

In a recent study of the $L1_2$ binaries and pseudobinaries, the occurrence/loss of the yield-stress anomaly was predicted[13] in all systems studied by considering the *necessary* condition for the stability of APB versus SISF and a *sufficient* condition for the stability of APB(111) versus (100) for cross-slip of screw dislocation segments. The APB and SISF energies, as well as c_{ij}, were obtained using DFT. The necessary and sufficient conditions were derived, respectively, by Paidar, Pope, and Yamaguchi[14] (modified by Liu *et al.*[13]) and Saada and Veyssiere.[15] The resulting stability map is applicable to any $L1_2$ material. Here, we adopt a similar approach. We construct two maps based on energy-stability criteria for competing slip modes in B2 structures that fully explain and predict enhanced ductility (or lack thereof) in B2 systems.

III. METHODS

DFT[16,17] calculations were performed to obtain required parameters of the theory. We employed the Vienna Ab Initio Simulation Package (VASP)[18–21] that uses pseudopotentials with a projector augmented wave (PAW) basis.[22,23] We adopted the generalized gradient approximation (GGA) to the exchange-correlation functional.[24,25] The lattice a and elastic c_{ij} constants were calculated for two-atom B2 cells with $20 \times 20 \times 20$ k-point meshes.[26] Total energies (forces) were converged below 0.1 meV/cell (1 meV/Å). Due to errors in GGA functionals, a for metals are overestimated ($a_{\mathrm{theory}} > a_{\mathrm{expt}}$ up to 1%), which affect the values c_{ij} and γ because the defect planes are farther apart and lowers the defect energy, giving material-dependent errors. Therefore, we used a_{expt} (if known) to create the maps to remove nonsystematic errors from calculated quantities. (The value of a_{expt} is unknown for YIn.) Note that removing such nonsystematic error is critical for predicting quantitatively other deformation processes, such as twinning,[27,28] because the atomic planes away from the planar defects are separated by geometric multiples of a_{expt} (the same distances as in experiment), but relaxation around the defects plane are included, so DFT provides a more correct shear surface energy.

The planar defect energies of APB$\{1\bar{1}0\}$ and SF$\{1\bar{1}0\}$ were calculated for 32-atom unit cells having at least $12 \times 12 \times 2$ k points. The APB$\{11\bar{2}\}$ was calculated using a 24-atom unit cell and $8 \times 8 \times 4$ k points. Examples of the various unit cells are shown in Fig. 2. The k-point meshes were chosen such that the reciprocal axes had a similar density of k points. The aspect ratio in k space, then, was roughly the reciprocal of that in real space. APBs and SFs on the $\{1\bar{1}0\}$ plane were separated by

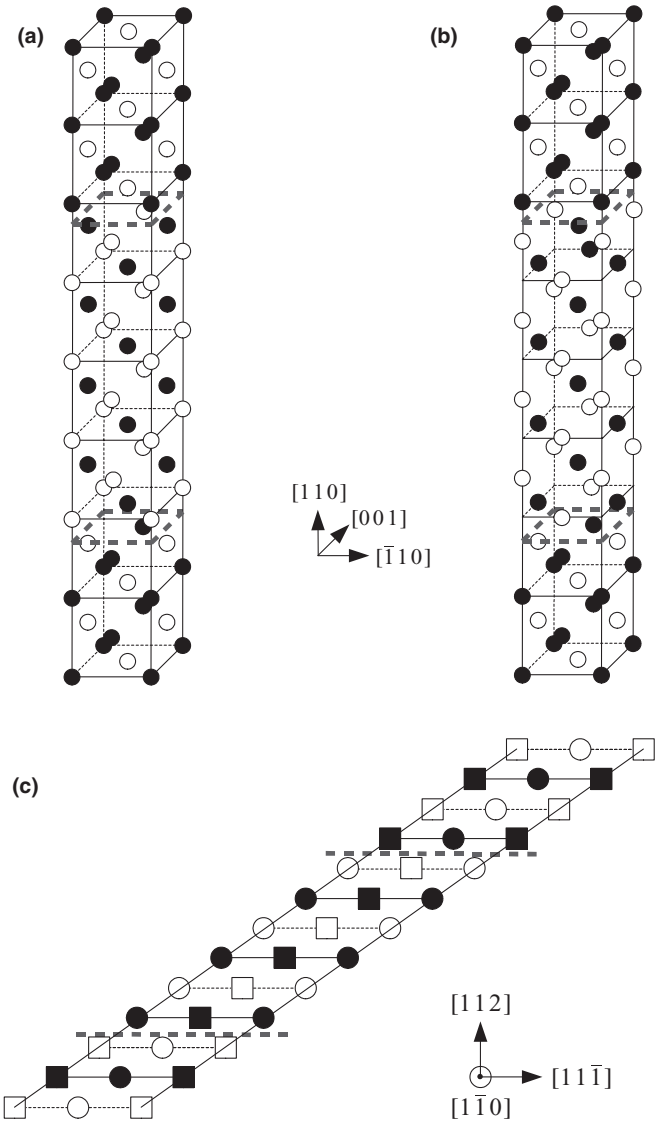

FIG. 2. Unit cells used for (a) APB$\{1\bar{1}0\}$, (b) SF$\{1\bar{1}0\}$, and (c) APB$\{11\bar{2}\}$. In (a) and (b), solid and open circles represent different atomic species. In (c), APB$\{11\bar{2}\}$ is projected onto the $(1\bar{1}0)$ plane. Solid symbols represent atoms in the plane; open symbols represent atoms $\frac{a}{2}[1\bar{1}0]$ behind the plane. The two defect planes per unit cell are represented by dashed lines.

eight layers of atoms, whereas APB$\{11\bar{2}\}$'s were separated by six layers. To remove errors for k-point meshes, the perfect cell had the same number of atoms and cell shape as the defective cell. (Note that defect planes may shift off their ideal lattice positions, an effect for which we have not accounted in the DFT results.) Defect energies were computed from

$$\gamma = \frac{E_{\text{defect}} - E_{\text{perfect}}}{m\|\mathbf{T}_1 \times \mathbf{T}_2\|} \tag{4}$$

for m defect planes per unit cell. Each unit cell contained two defect planes, so that orthogonal translation vectors $\mathbf{T}_{1,2,3}$ could be used as coordinate axes along the defect plane. In defective cells, two layers of atoms on each side of the defect plane were relaxed along $\mathbf{T}_3$, with the cell shape and volume fixed to remove systematic errors. Specifically, the translation vectors were

$$\frac{1}{a}\begin{bmatrix}\mathbf{T}_1\\ \mathbf{T}_2\\ \mathbf{T}_3\end{bmatrix} = \begin{cases}\begin{bmatrix}\bar{1} & 1 & 0\\ 0 & 0 & 1\\ 8 & 8 & 0\end{bmatrix} & \text{APB and SF}\{1\bar{1}0\}\\ \begin{bmatrix}\bar{1} & 1 & 0\\ \bar{1} & \bar{1} & 1\\ 2 & 2 & 4\end{bmatrix} & \text{APB}\{11\bar{2}\}\end{cases}. \tag{5}$$

Following Mehl *et al.*,[29] we obtained the necessary elastic constants c_{ij} by solving for c_{44}, $c' = (c_{11} - c_{12})/2$, and bulk modulus $B = (c_{11} + 2c_{12})/3$ through appropriate lattice distortion, where the Zener ratio $A = c_{44}/c'$ and $G = c_{44}$. The total energy for each strain distortion in B2 is proportional to ϵ^2, with $O(\epsilon^4)$ error, giving more accurate coefficients. The Poisson ratio in Table I is computed from

$$\nu = \frac{3B - 2G}{6B + 2G}. \tag{6}$$

We provide in Table I the DFT and known observed values of all required quantities that are necessary in the maps that indicate enhanced ductility using elastic properties and relative defect energies.

IV. NECESSARY AND SUFFICIENT CONDITIONS FOR B2 DUCTILITY

We now derive the two conditions for ductility, applying them in Sec. V. Multiple slip can occur via formation of $\langle 111\rangle$ APBs on the $\{1\bar{1}0\}$ and $\{11\bar{2}\}$ planes. (For simplicity, the $\frac{a}{2}\langle 111\rangle\{1\bar{1}0\}$ and $\frac{a}{2}\langle 111\rangle\{11\bar{2}\}$ APBs and $\frac{a}{2}\langle 001\rangle\{1\bar{1}0\}$ SFs are denoted as APB$\{1\bar{1}0\}$, APB$\{11\bar{2}\}$, and SF$\{1\bar{1}0\}$.) It is necessary, then, that the $\langle 111\rangle$ APBs have to be more energetically favorable than the $\langle 001\rangle$ SFs. To predict $\langle 111\rangle$ versus $\langle 001\rangle$ slip, Rachinger and Cottrell[44] gave a simple criterion in terms of width of APB: If $w_{\text{APB}}/a \gg 1$, then $\langle 111\rangle$ slip is favorable; else if $w_{\text{APB}}/a \approx 1$, then $\langle 001\rangle$ is favorable. We have derived a more quantitative necessary condition[45] (see Appendix A) in light of Paidar, Pope, and Yamaguchi's work in $L1_2$ systems.[14]

Saada and Veyssiere[39] investigated the sufficient condition for cross-slip of a $\langle 111\rangle$ screw superdislocation on $\{1\bar{1}0\}$ and $\{11\bar{2}\}$ planes that leads to multiple-slip systems. The possible dissociation mechanisms for a $\langle 111\rangle$ screw superdislocation are

$$\begin{aligned} a\langle 111\rangle &\to a\langle 110\rangle + a\langle 001\rangle \\ &\to a\langle 100\rangle + a\langle 010\rangle + a\langle 001\rangle, \qquad (7a)\\ a\langle 001\rangle &\to \frac{a}{2}\langle 001\rangle + \text{SF} + \frac{a}{2}\langle 001\rangle, \qquad (7b)\\ a\langle 111\rangle &\to \frac{a}{2}\langle 111\rangle + \text{APB} + \frac{a}{2}\langle 111\rangle. \qquad (7c)\end{aligned}$$

In Eq. (7a), the $\langle 111\rangle$ screw dislocation can further dissociate into perfect dislocations along the cube edges (Fig. 1); hence, there are no APBs or SFs. Equation (7b) involves formation of SFs.

A. Necessary condition

As described above, there are two criteria that must be met simultaneously that provide the *necessary* condition for ductility: $\langle 001\rangle$ should be the dominant slip direction, yet $\langle 111\rangle$ slip should also be possible with formation of $\langle 111\rangle$ APBs; see Fig. 1. An overview of the derivation is provided in Appendix A.

On purely energetic grounds, for B2 materials to possess multiple slip during plastic flow, $\langle 001\rangle\{1\bar{1}0\}$ slip must be more favorable than $\langle 111\rangle\{1\bar{1}0\}$ slip via APB$\{1\bar{1}0\}$ formation, which occurs[45] (see Appendix A) if

$$w_{\text{APB}} \leqslant kea \sim 5.9a \quad \text{or} \tag{8a}$$

$$\ln C \geqslant -3.9. \tag{8b}$$

Equation (8) justifies the criterion imposed by Rachinger and Cottrell[44] and gives a fixed measure across B2 systems. The second form is useful for presenting the maps.

Now, to have enhanced ductility, both $\langle 001\rangle$ as the dominant slip direction, and $\langle 111\rangle$ slip also possible by formation of $\langle 111\rangle$ APBs, the APBs must be more energetically favorable than SFs. The key *necessary* condition[45] (see Appendix A), using Eqs. (2) and (3), is

$$\delta > 0.119C^{-1/4} \quad \text{or} \tag{9a}$$

$$\ln\delta > -2.132 - \tfrac{1}{4}\ln C, \tag{9b}$$

where the second form is easier for plotting the maps. Together Eqs. (8) and (9) constitute the map for B2 systems that will have both dominant $\langle 001\rangle$ slip and $\langle 111\rangle$ slip due to formation of APBs.

For our generic map and necessary conditions, as a standard simplification, we used a Poisson ratio of 1/3 (not values in Table I), which yields integer coefficients related to ν. We also used an effective dislocation interaction range of twice the core width ($r = 2r_0 = 2ka$; see Appendix A). While $\nu = 1/3$ and the estimated k simplifies the algebra for the maps, the reader should appreciate that the exact borders for each material can be shifted by the actual values—the price for a generic map; hence, borderline cases should be assumed possibly relevant. Also, differences in various DFT calculations could alter locations in the maps, as we show explicitly.

B. Sufficient condition

As noted earlier, a ductile B2 material can have multiple slip only if APBs have bistable existence on both $\{1\bar{1}0\}$ and

TABLE I. Calculated and observed B2 lattice constants (a in Å), bulk modulus (B in GPa), and elastic constants (c_{ij} in GPa). A, ν, and M are defined in the main text. In the first (second) row of each system, DFT calculations were performed at a_{DFT} (a_{expt}). References for a_{expt} are given in the second row. In the third row, B, c', A, ν, and M were derived from the experimental elastic constants. Dashes indicate that no data are available.

Material	a	B	c'	c_{11}	c_{12}	c_{44}	A	ν	M	Ref.
YAg	3.646	68.3	22.3	98.0	53.4	35.0	1.57	0.281	1.02	
	3.619	75.1	22.6	105.2	60.0	37.8	1.67	0.284	1.02	10
	3.619	70.1	24.2	102.4	54.0	37.2	1.54	0.276	1.02	10
YCu	3.485	71.3	34.4	117.2	48.4	36.4	1.06	0.282	1.00	
	3.477	73.4	34.6	119.6	50.3	37.2	1.08	0.283	1.00	10
	3.477	70.1	32.5	113.4	48.4	32.3	0.99	0.300	1.00	10
YIn	3.769	57.3	6.02	65.3	53.3	43.4	7.20	0.198	1.35	
	–									
	–									
YRh	3.442	113.3	38.4	164.5	87.7	36.6	0.95	0.354	1.00	
	3.407	121.2	38.0	171.8	95.9	40.4	1.06	0.350	1.00	30
	–									
YMg	3.798	41.2	8.62	52.7	35.5	39.6	4.60	0.136	1.19	
	3.806	40.4	8.55	51.8	34.7	39.1	4.57	0.134	1.18	31
	–									
YZn	3.578	62.6	22.6	92.7	47.5	43.2	1.92	0.219	1.03	
	3.577	62.8	22.6	92.9	47.7	43.3	1.92	0.219	1.03	32
	–									
ScAg	3.422	87.7	20.4	114.9	74.1	47.1	2.31	0.272	1.06	
	3.412	91.2	20.7	118.8	77.4	48.5	2.34	0.274	1.06	33
	–									
ScAu	3.393	111.9	25.3	145.7	95.0	47.4	1.87	0.314	1.03	
	3.369	123.7	26.1	158.5	106.3	51.8	1.98	0.316	1.04	34
	–									
ScCu	3.245	96.1	37.5	146.2	71.1	54.8	1.46	0.261	1.01	
	3.257	91.5	36.8	140.4	67.1	52.8	1.44	0.258	1.01	35
	–									
ScPd	3.301	119.9	32.8	163.5	98.0	42.8	1.31	0.341	1.01	
	3.283	128.8	33.2	173.1	106.6	45.5	1.37	0.342	1.01	33
	–									
ScPt	3.293	146.9	28.7	185.1	127.8	49.8	1.74	0.348	1.03	
	3.268	162.8	28.4	200.7	143.8	54.9	1.93	0.348	1.04	36
	–									
ScRh	3.218	149.6	62.1	232.4	108.3	51.8	0.84	0.345	1.00	
	3.206	157.3	63.5	242.0	114.9	54.0	0.85	0.346	1.00	33
	–									
ScRu	3.201	152.5	77.1	255.4	101.1	40.4	0.52	0.378	1.04	
	3.203	151.2	76.8	253.6	100.0	40.0	0.52	0.378	1.04	33
	–									
NiAl	2.895	159.4	38.4	210.5	133.8	112.8	2.94	0.214	1.10	
	2.886	166.0	39.5	218.7	139.6	116.5	2.95	0.216	1.10	37
		166.0	34.2	211.6	143.2	112.1	3.28	0.224	1.12	38
FeAl	2.879	161.3	52.8	231.6	126.1	130.2	2.47	0.182	1.06	
	2.909	156.4	51.7	225.4	121.9	123.5	2.39	0.187	1.06	37
		136.1	33.7	181.1	113.7	127.1	3.77	0.144	1.14	38
AuCd	3.398	93.0	1.31	94.7	92.1	37.4	28.8	0.323	2.41	
	3.323	130.8	1.58	132.9	129.8	56.1	36.2	0.312	2.66	37
		85	3.5	90	83	44	12.6	0.279	1.68	39
AuZn	3.195	116.9	5.72	124.5	113.1	42.8	7.47	0.337	1.42	
	3.149	145.4	7.31	155.2	140.5	55.7	7.62	0.330	1.42	40
	3.149	131.5	7.73	141.8	126.3	54.52	7.04	0.318	1.38	40

TABLE I. (*Continued.*)

Material	a	B	c'	c_{11}	c_{12}	c_{44}	A	ν	M	Ref.
CuZn	2.969	113.8	7.67	124.0	108.7	78.6	10.2	0.219	1.53	
	2.954	122.6	8.00	133.3	117.3	83.5	10.4	0.222	1.54	37
		116.2	9.70	129.1	109.7	82.4	8.50	0.213	1.43	41
AgMg	3.331	65.9	13.4	83.8	57.0	47.1	3.51	0.212	1.13	
	3.314	70.9	14.2	89.8	61.5	49.7	3.51	0.216	1.13	37
		65.6	13.7	83.8	56.4	47.6	3.46	0.208	1.13	38
CsCl	4.196	15.0	11.0	29.6	7.65	5.24	0.48	0.344	1.04	
	4.120	19.3	11.6	34.7	11.6	8.03	0.69	0.317	1.01	42
		18.2	14.0	36.6	8.82	8.04	0.58	0.307	1.02	38
CsI	4.656	10.0	7.01	19.4	5.37	4.20	0.60	0.316	1.02	
	4.567	13.2	7.54	23.3	8.21	6.56	0.87	0.287	1.00	42
		12.7	8.95	24.6	6.70	6.24	0.70	0.289	1.01	38
TlBr	4.011	22.1	12.6	38.9	13.7	6.21	0.49	0.372	1.04	
	3.986	24.4	12.7	41.3	15.9	7.51	0.59	0.360	1.02	43
		22.4	11.2	37.3	14.0	7.48	0.67	0.350	1.01	38
TlCl	3.855	25.6	14.5	44.9	16.0	7.11	0.49	0.373	1.04	
	3.842	27.0	14.5	46.4	17.3	7.86	0.54	0.367	1.03	43
		23.6	12.4	40.1	15.3	7.60	0.61	0.355	1.02	38

$\{11\bar{2}\}$ planes (see Fig. 1)—this is the *sufficient* condition. Following Head[46] and Hirth and Lothe,[47] the dissociation of $\langle 111\rangle$ B2 screw superdislocations was analyzed by Saada and Veyssiere,[39] and expanded on by Sun,[48] in terms of the relative energetics of those planes,

$$\lambda \equiv \gamma_{\mathrm{APB}}^{11\bar{2}} / \gamma_{\mathrm{APB}}^{1\bar{1}0}, \tag{10}$$

and a ratio of S_{ij} elements

$$M = \sqrt{\frac{S_{11}S_{44}}{S_{11}S_{44} - S_{15}^2}}. \tag{11}$$

See Ref. 47 for the full derivation of M and the definition of S_{ij}, which are obtained by a rotation of the c_{ij} from cubic axes to the $\langle 111\rangle$ axis, as we also present in Appendix B. To satisfy the sufficient condition, expressed in terms of a dimensionless map (λ versus M), the λ must be strictly bounded as[48]

$$\frac{\sqrt{3}}{2} \leqslant \lambda \leqslant \frac{2}{\sqrt{3}}. \tag{12}$$

Within this bound, Sun found[48] that both slip directions are active, but $(1\bar{1}0)$ is dominant for $M^{1/3} < \lambda < 2/\sqrt{3}$ while $(11\bar{2})$ is dominant for $\sqrt{3}/2 < \lambda < M^{1/3}$.

C. Prediction from combined maps

As the major results, we now have the necessary and sufficient conditions for enhanced B2 ductility. First, our more quantitative "Rachinger-Cottrell" criterion, Eq. (8), is used to predict dominant $\langle 001\rangle$ slip. Then, on the same map, Eq. (9) compares the relative stability of APB$\{1\bar{1}0\}$ and SF$\{1\bar{1}0\}$ so that, if APBs are favorable, the systems possessing both $\langle 001\rangle$ and $\langle 111\rangle$ slip directions satisfy the necessary condition for ductility. Second, multiple slip in $\{1\bar{1}0\}$ and $\{11\bar{2}\}$ via APB formation is governed by the sufficient condition [Eq. (12)] in a second map. Practically, if the necessary condition is fulfilled (the first map), then the sufficient condition is checked (the second map) for whether the material possesses bistability of APBs, and, hence, multiple slip can occur for enhanced ductility. We now use these to predict ductility for several B2 systems.

V. RESULTS

A. Necessary condition

A necessary condition map is constructed in Fig. 3. The dimensionless ratios C and δ are defined in Eqs. (2) and (3), respectively. From Eq. (10) in Appendix A, it is shown that

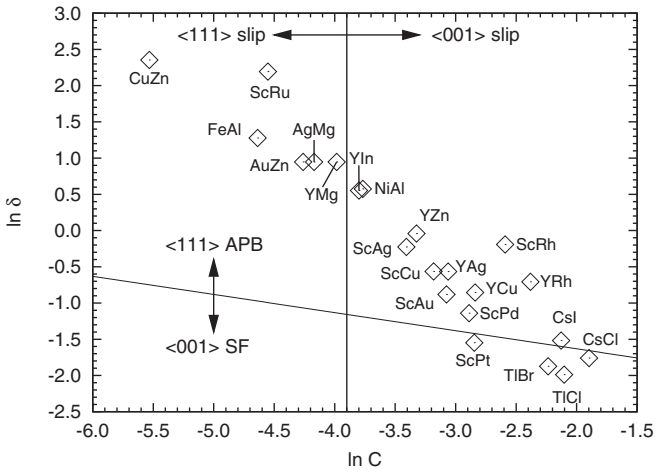

FIG. 3. Necessary condition ($\ln\delta$ versus $\ln C$ map) for preferred slip and APB/SF stability. To the right (left) of the vertical line, $\langle 001\rangle$ ($\langle 111\rangle$) slip is more favorable. Above the slanted line, APBs are more stable than SFs. Systems in the upper-right region satisfy the necessary condition for ductility. Note the data shown lie roughly along a line of slope slightly less than -1.

Eq. (8) can be expressed in terms of C. This condition translates to the vertical line drawn in Fig. 3, where ⟨001⟩ slip (⟨111⟩ slip) is more favorable for systems lying to the right (left). Equation (9) translates to the slanted line in Fig. 3. Therefore, the necessary condition is satisfied in the upper-right region defined by these two lines, in which ⟨001⟩ is the dominant slip direction and formation of APBs, rather than SFs, is preferred. We note that the data in Fig. 3 lie along a line of slope slightly less than −1.

Systems favoring ⟨001⟩ slip include all the ionic compounds, all the Y-based compounds except for YMg, all the Sc-based compounds except for ScRu, and NiAl. Notably, ScPt is ductile[2] but just barely predicted to be brittle from our analytic necessary conditions, a result that does depend on the accuracy of the DFT-derived inputs, or the underlying simplifications. For example, ScPt in Fig. 3 does satisfy the necessary conditions if $k \approx 4$ (rather than the $k = 2.17$ we assumed for all alloys, but it is in the acceptable range; see Appendix A). For $k \approx 4$, the APB versus SF slanted line shifts slightly down but parallel to the $k = 2.17$ line and ScPt falls in the upper-right region.

Ionic compounds are expected to exhibit ⟨001⟩ slip because ions encounter lower charge repulsion as they slip along cubic edges rather than cube diagonals. CuZn and FeAl fall on the left-hand side of the vertical line, showing that ⟨111⟩ slip is favorable, agreeing with their observed exclusive ⟨111⟩ slip.[44,49–52] Interestingly, both ⟨111⟩ slip[44] and ⟨001⟩ slip[53] have been observed in AgMg, with a transition from ⟨111⟩ to ⟨001⟩ slip at low temperatures.[6] For AuZn ($A \sim 7.5$), the predicted ⟨111⟩ slip does not agree with the reported ⟨001⟩ slip[44,53] and further investigation is required. From Table I the largest errors in our calculated elastic constants are found in AuCd; we have omitted it from our ductility maps. The discrepancies observed in the two Au compounds may be caused by the usage of nonrelativistic pseudopotentials. It has been shown that relativistic effects play an important role in the bonding of Au clusters[54] and may also pertain to the study of bulk compounds. For all the other systems, our simple model predicts ⟨001⟩ versus ⟨111⟩ slip accurately.

Figure 3 also compares the relative stability of SF$\{1\bar{1}0\}$ and APB$\{1\bar{1}0\}$. For the ionic compounds, SFs are more stable than APBs. Charge repulsion in the APB is much higher than that in the SF. (See Table II for the calculated planar defect energies.) On the other hand, APBs are relatively stable in both the Y-based compounds and the classic B2 alloys.

Systems in the upper-right region, as defined by the vertical and slanted lines, of Fig. 3 satisfy the *necessary* condition for ductility. In this region, ⟨001⟩ slip is favorable but ⟨111⟩ APBs are stable, which means that $\frac{a}{2}\langle 111\rangle$ partial dislocations can coexist with the ⟨111⟩-dissociated perfect ⟨001⟩ dislocations. Indeed, it has been reported[59] that ⟨111⟩ dislocations are metastable in NiAl and that they have been observed in the Y-based compounds.[1]

The *first central finding* is that the B2 stability map in Fig. 3 identifies candidates for multiple slip, and only a subset of Y- and Sc-based systems and some others qualify, namely, YAg, YCu, YIn, YRh, YZn, ScAg, ScAu, ScCu, ScPd, (ScPt), ScRh, NiAl, CsI, and (CsCl), where the parentheses reflect a borderline case that should be checked.

B. Sufficient condition

The *necessary* condition alone cannot predict ductility. The *sufficient* condition (Fig. 4)—whether the APBs are bistable on $\{1\bar{1}0\}$ and $\{11\bar{2}\}$ planes—must be verified. Dimensionless ratios λ and M are defined in Eqs. (10) and (11), respectively. The condition for bistability of APBs is satisfied in regions II and III, according to Eq. (12). In region II, the $\{1\bar{1}0\}$ APB has lower energy, and vice versa in region III (see Fig. 4).

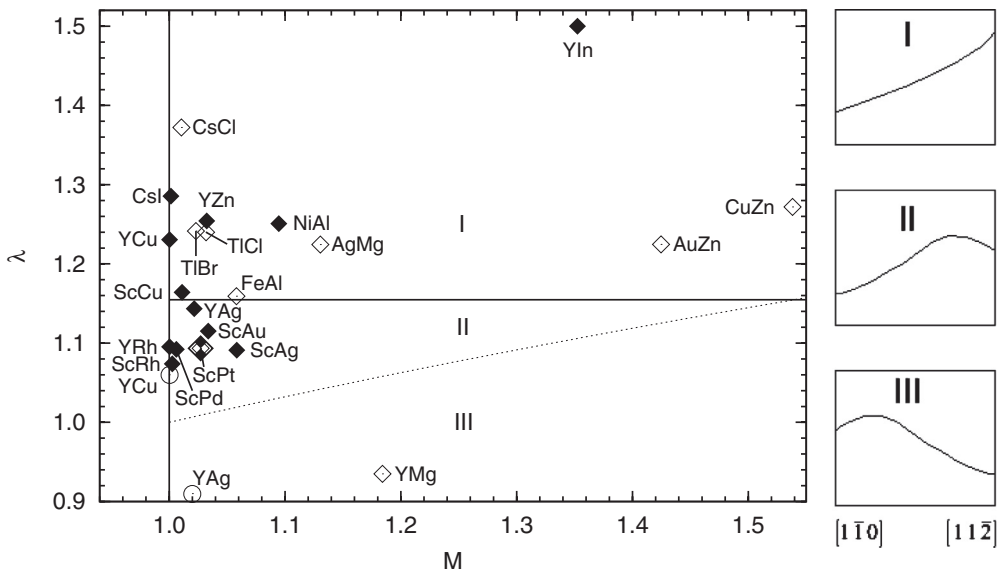

FIG. 4. Left: Sufficient condition (λ versus M) map for multiple slip systems [Eq. (12)] that occurs if $\sqrt{3}/2 < \lambda < 2/\sqrt{3}$. Materials not satisfying the *necessary* condition are marked by open diamonds. ScPt, being the borderline case in Fig. 3, is marked by a half-filled diamond. DFT values of YCu and YAg reflecting energies from Ref. 10 are indicated by open circles. Right: Schematics showing the relative energy of the slip systems (after Ref. 48). Below $\lambda = \sqrt{3}/2 \approx 0.866$, only $\{11\bar{2}\}$ slip is favored.

TABLE II. Calculated B2 APB and SF energies (in mJ/m^2). The dimensionless parameters C, δ, λ, and M are defined in Eqs. (2), (3), (10), and (11), respectively. Calculated results are listed in the first row of each system. Other calculated results of γ_{APB} and γ_{SF} are provided, if available.

Material	$\gamma_{APB}^{1\bar{1}0}$	$\gamma_{APB}^{11\bar{2}}$	λ	$w_{APB}^{1\bar{1}0}/a$	C	Ref.	$\gamma_{SF}^{1\bar{1}0}$	δ	Ref.
YAg	641	732	1.14	2.55	0.0468		364	0.569	
	745	680	0.91	2.16	0.0553	10	305	0.409	55
YCu	757	931	1.23	2.04	0.0585		322	0.425	
	1030	1090	1.06	1.30	0.0917	10	270	0.262	55
YIn	366	549	1.50	5.33	0.0224		636	1.740	
							480		55
YRh	1270	1390	1.10	1.29	0.0924		626	0.493	
							430		55
YMg	277	259	0.93	6.41	0.0186		714	2.58	
YZn	558	700	1.25	3.31	0.0360		536	0.961	
ScAg	548	598	1.09	3.60	0.0331		437	0.797	
ScAu	805	898	1.12	2.59	0.0461		333	0.414	
ScCu	713	830	1.16	2.88	0.0415		406	0.569	
ScPd	832	908	1.09	2.14	0.0557		266	0.320	
ScPt	1042	1139	1.09	2.05	0.0581		222	0.213	
ScRh	1296	1392	1.07	1.59	0.0749		1069	0.825	
ScRu	135	506	3.74	11.3	0.0105		1213	8.967	
NiAl	777	971	1.25	5.17	0.0231		1379	1.77	
	815	995	1.22	4.74	0.0252	10	1290	1.58	10
	810	990	1.22	4.93	0.0250	56			
FeAl	348	403	1.16	12.3	0.0097		1248	3.59	
	300	820	2.73	14.7	0.0081	56			
AuCd	187	223	1.19	11.9	0.0101		639	3.41	
AuZn	247	303	1.22	8.47	0.0141		636	2.58	
CuZn	98	124	1.27	30.2	0.0040		1027	10.5	
	50	37	0.74 (1.09)	58.1	0.0021	57[a] (58[a])			
AgMg	254	311	1.22	7.73	0.0154		655	2.58	
CsCl	496	659	1.33	0.80	0.1500		85	0.172	
CsI	357	459	1.29	1.00	0.1191		78	0.219	
TlBr	320	397	1.24	1.12	0.1069		49	0.154	
TlCl	369	458	1.24	0.98	0.1221		51	0.137	

[a]Experiment.

In regions I ($\lambda > 2/\sqrt{3}$) and IV ($\lambda < \sqrt{3}/2$, not shown), respectively, $\{11\bar{2}\}$ and $\{1\bar{1}0\}$ APBs are unstable. ScRu is not shown as its λ value falls out of range (Table II). ScCu satisfies the necessary condition and just barely does not satisfy the sufficient conditions; this borderline case is sensitive to DFT approximations. For example, a 1.4% increase in the $\gamma_{APB}^{1\bar{1}0}$, i.e., from 713 to 723 mJ/m^2, in Table II would put ScCu below the bistability line; hence, we include ScCu as ductile. The compounds that satisfy both the necessary and sufficient conditions are YAg, YRh, ScAu, ScAg, (ScPt), ScPd, (ScCu), and ScRh. For these B2 materials we predict enhanced ductility; all other compounds are predicted to be brittle.

Out of all the B2 systems, only YAg and YCu have been examined in other DFT calculations.[10] There are two notable things: (1) elastic constants in Table I from our and Morris *et al.*'s results are the same and agree with experiment, but (2) the defect energies are significantly different in Table II. We have been unable to reproduce their defect energies for YCu, and for YAg the values are similar but swapped, changing the relative energies λ in Fig. 4. If Morris *et al.*'s λ values for YCu and YAg are plotted in Fig. 4, their locations both shift downward, with YCu (YAg) now in region II (III), and both (not just YAg) satisfy bistability explaining enhanced ductility.

The *second central finding* is that the sufficient condition shown in Fig. 4 identifies B2 materials that can exhibit multiple slip. Systems that do not satisfy the necessary condition are included for comparison. Only YAg, [YCu], YRh, ScAu, ScAg, (ScPt), ScPd, (ScCu), and ScRh possess $\{1\bar{1}0\}$ and $\{11\bar{2}\}$ bistability, while other candidates lie away from the bistability region. Bracketed YCu reflects the unresolved DFT values. The bistability of APBs explains the observation of many $\langle 111\rangle$ dislocations in the ductile Y-based[1] and Sc-based compounds, even though $\langle 001\rangle$ is the dominant slip direction.

VI. DISCUSSION

The systems that satisfy the *necessary conditions* (Fig. 3 showing dominant $\langle 001\rangle$ slip existing with $\langle 111\rangle$ slip and stable APBs, not SFs) and the *sufficient condition* (Fig. 4, regions II and III, showing APBs having bistable slip) are predicted to

have significant enhanced ductility unexpected in B2 systems. Borderline cases (if using DFT inputs) should be carefully addressed. It happens that none of the elastically anisotropic B2 materials satisfy both the necessary and sufficient conditions, explaining the observation of brittleness in all the classic B2 alloys, which are anisotropic.[7] The ductile materials are all nearly isotropic. Hence, elastic isotropy ($A \sim 1$) should serve as an indicator for enhanced ductility. It is, however, not a quantitative indicator because YCu is more isotropic than YAg, but YCu is less ductile.

ScRu is predicted to be brittle, which agrees with experiment.[2] ScAg, ScAu, and ScPd are correctly predicted to be ductile. ScPt is ductile[2] but is a borderline case barely not satisfying the necessary condition. And, if we take ScPt to satisfy the necessary condition, then it is ductile because the sufficient condition is also satisfied. (If ScPt is taken to satisfy necessary condition, then so too should CsCl, but it does not satisfy the sufficient condition.) The Rh compounds YRh and ScRh are brittle[2] but predicted to be ductile. Further investigation in this chemical space is required to understand the source of the discrepancy. As noted, the neglect of a shift of the defect planes from the ideal position, the sensitivity to the specific DFT exchange-correlation functional, or the neglect of other defect formations may change these cases.

Not all Y-based compounds are predicted to be ductile: B2 YIn does not satisfy the sufficient condition (similar to AuZn, $A \sim 7.5$, which means that it is not very isotropically elastic); YMg does not satisfy the necessary condition, so it is brittle, as found experimentally.[5] YIn has been observed to form a B2 phase.[60,61] However, YIn has been reported to crystallize also into a tetragonal phase,[62] which is ductile. Our DFT calculations (unpublished) show that YIn has a shallow energy trough versus c/a making it susceptible to c/a distortion depending on sample treatment. Thus, while the B2 YIn is brittle from our theory for B2 ductility (using our DFT results), if c/a distortion occurs, a more general ductility criterion for the dislocation-defect reactions should be derived accounting for c/a dependence.

Finally, regarding correlation of measured ductility with d-electron density of states (DOS), we note that our theory addresses the ductility criterion based on defect energies and elastic constants that inherently reflect the bonding represented within DFT, as did the theory of Liu *et al.* on yield-strength anomalies in $L1_2$ compounds.[13] A similar approach for quantitative prediction of twinning in elements and solid-solution alloys (based on the interacting dislocation and planar-defect arrays in a twin nucleus) also reflect bonding, which can be correlated directly to the electronic structure.[28] As noted above, a significant (but not absolute) correlation of calculated d-electron DOS at the Fermi energy was cited for B2 alloys that were measured to have little to no ductility.[2] Importantly, from our maps for the necessary and sufficient conditions (using our DFT results), we can predict ductility and, if desired, attempt to correlate behavior with the DFT-derived DOS.

In Fig. 5, we show the DOS for B2 ScRu (brittle), ScRh (predicted ductile, observed brittle), and ScPd and ScAg (both ductile) in order of increasing electron-per-atom ratio, or e/a. ScRu has the largest d-state DOS at the Fermi level and correlates with the predicted/observed lack of ductility. ScRh, with its extra electron over ScRu, is in low-d-state DOS between bonding and antibonding d states, which suggests a crossover in bonding behavior—not incompatible with the present results taken *in toto*. Both ScPd and ScAg are ductile, with the Fermi energy beginning to climb into higher d-band DOS and the bonding peak of the d-band DOS falling farther below the Fermi energy. These results appear to agree with the results of Gschneidner *et al.*,[2] but their DOS contains no detail to make any direct comparison. They argue only that a broad d-band DOS at the Fermi energy explains the lack of ductility, whereas, for ScPd and ScAg, this d-band feature is farther below the Fermi energy and accounts for ductility; how it does so is not explained. Of course, that the Fermi energy is entering the DOS with antibonding character should make ductility, i.e., defect formation, more energetically favorable, as inherently represented in the present theory. We can correlate our predicted brittleness, brittle-to-ductile crossover, and ductility with the change in DOS features. Thus, we agree that the magnitude of the d-band DOS at the Fermi energy can be correlated with ductility if already known, but such a correlation by itself is not predictive theory. Indeed, the change in DOS under shear is more relevant, as is known for aluminum;[63] for example, s bonds under shear become very directional, giving rise to a large stacking fault energy, as observed. Hence, investigating the behavior of the charge density under shear may be more fruitful than DOS.

Finally, for completeness, we note that the underlying theory for higher ductility is generally more complicated than the simple dissociations present here as a starting analysis. That is, there are key factors determining slip systems, e.g., elastic anisotropy, the "correct" vectors of possible faults in (101) planes (not always corresponding to the usually presumed APBs), and the energies of these faults. So, it is possible that the splittings could be different from the usual APBs considered here. As a starting point, if all B2 systems are treated equally, we assume that there are well-defined APBs on $\{1\bar{1}0\}$ and $\{11\bar{2}\}$ planes with the displacement vector $\frac{1}{2}\langle 111\rangle$ and also a stacking fault on $\{1\bar{1}0\}$ planes with the vector $\frac{1}{2}\langle 001\rangle$. However, the existence of such metastable faults is by no means guaranteed—indeed they are system specific. The metastability of such faults is the crucial condition for any further considerations employing standard (anisotropic) dislocation theory. The symmetry does not provide a guarantee of the stability of these faults. On $\{1\bar{1}0\}$ planes there may be metastable $\frac{1}{2}\langle 111\rangle$ faults in some materials, e.g., CuZn or FeTi.[64] However, the vectors corresponding to metastable faults may differ from $\frac{1}{2}\langle 111\rangle$; for example, simulations using empirical potentials found in NiAl that the APB with $\frac{1}{2}\langle 111\rangle$ is not actually stable but other faults on $\{1\bar{1}0\}$ planes existed.[65] The point is that vectors of the faults on $\{1\bar{1}0\}$ planes vary from material to material and are by no means the same in all B2 compounds.

Nonetheless, the present stability analysis provides a very rapid analysis to identify and reduce the number of candidate anomalously ductile B2 systems, and, from which, one can consider other, more atypical, instabilities. For future work, we can investigate the metastability of the planar defects addressed in the present simplest theory, since they may be unstable with respect to other defects on the activated slip planes. If so, the dissociation mechanisms considered here would then be

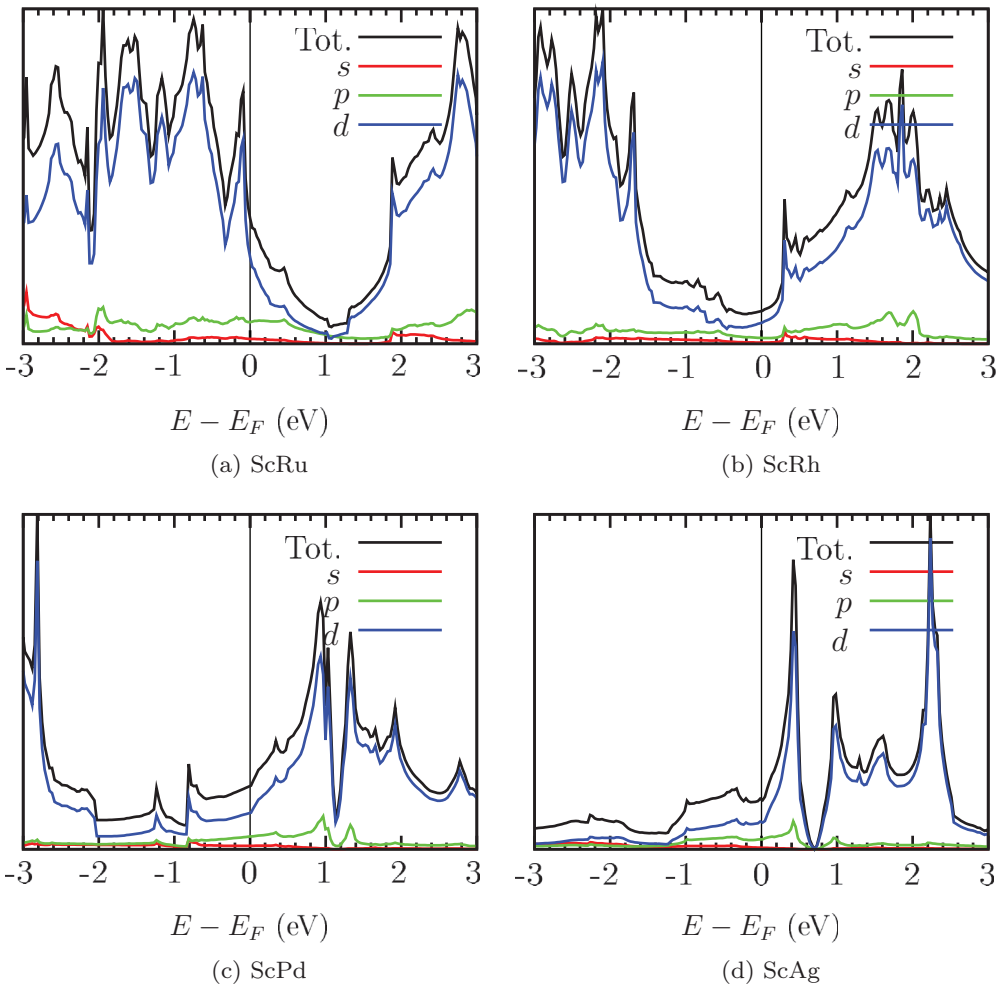

FIG. 5. (Color online) Electronic DOS [relative to Fermi energy E_F (in eV), in arbitrary units] for B2 Sc-based alloys in order of (a) Ru, (b) Rh, (c) Pd, and (d) Ag, i.e., increasing e/a. ScRu is predicted/observed to be brittle, ScPd and ScAg are predicted/observed to be ductile, and, at the crossover, ScRh is predicted to be ductile but observed to be brittle.

altered, possibly changing the maps and predictions, which, nonetheless, already appear highly accurate.

VII. CONCLUSIONS

Through solely energy-based criteria for ductility (dislocation and defect formation), we have addressed ⟨001⟩ versus ⟨111⟩ slip, the relative stability of APBs and SFs, and the bistability of APB$\{1\bar{1}0\}$ and $\{11\bar{2}\}$, which are the dominant slip modes and defects in B2 systems that can lead to enhanced ductility. Through these criteria, we have provided a set of stability maps requiring only ratios of defect energies and/or elastic constants, obtained here from DFT calculations. For design, these maps determine *a priori* whether a B2 material is brittle or ductile and indicate typical versus enhanced ductility. These maps explain and predict the enhanced ductility observed (or lack thereof) in RM intermetallic compounds. One may consider temperature effects, point defects, or disorder to modify the maps for system-specific predictions, as well as more system-specific superdislocation reactions that we did not consider.

We have examined 23 B2 materials, some of which show dramatically enhanced ductility, comparable to fcc aluminum. For B2 materials, ⟨001⟩ slip is more favorable than ⟨111⟩ if the width of APB$\{1\bar{1}0\}$ is less than $6a$. To summarize our results from the B2 stability maps:

(1) For ionic compounds, only ⟨001⟩ slip is possible, as the necessary condition for ductility is not satisfied. If the borderline CsI were assumed to satisfy the necessary condition, the lack of APB bistability would account for its brittleness.

(2) For classic B2 alloys, all but NiAl fail the necessary condition. Again, APBs of NiAl do not possess bistability (multiple slip) so there is no increased ductility.

(3) For Y- and Sc-based compounds, YAg, YRh, ScAg, ScAu, (ScPt), ScPd, (ScCu), and ScRh satisfy both conditions for multiple-slip systems. Thus, we predict them to exhibit high ductility (observed for YAg). YIn and YMg do not satisfy either condition, so they are predicted to be brittle (observed in YMg), while B2 YIn has competing tetragonal distortions that will affect prediction.

(4) We predicted some systems, such as ScRh, that are ductile but brittle; these appear at a crossover, e.g., between ScRu

(brittle) and ScPd (ductile) correctly predicted, suggesting the more detailed dislocation reaction or computational details may be at issue, not the general theory.

Overall the results are in very good agreement with experiment and, if desired, can be correlated directly with the underlying electronic-structure details, as done with other similar theories for yield-strength anomalies in $L1_2$ compounds or twinning in fcc metals, because the theory inherently contains all the bonding information within the defect energy and elastic constants that are needed.

In closing, an energy-based mesoscale dislocation analysis combined with first-principles calculations accurately characterizes permitted slip modes in B2 systems and predicts enhanced ductility due to coexistence of $\langle 001\rangle$ slip and $\langle 111\rangle$ APBs, and bistability of APBs on $\{1\bar{1}0\}$ and $\{11\bar{2}\}$ planes. The Zener anisotropy ratio can be used to screen candidates for further investigation via these stability maps. Given that ductility is such a complex phenomenon at the atomistic level, it is remarkable that our ductility model (with some simplifying assumptions) and associated necessary and sufficient conditions give fairly accurate predictions by simply considering dissociation energies of a single superdislocation and the planar energies of the resulting defects.

ACKNOWLEDGMENTS

We thank Karl Gschneidner, Jr. and James Morris for sharing their results, respectively, on YMg and B33 versus B27 stability. We thank Vaclav Vitek for discussions on complexities for more general theory. Funding was from the Department of Energy, Basic Energy Sciences, Division of Materials Science and Engineering (Grant No. DEFG02-03ER46026) and "materials discovery" seed funding in Ames. The research was performed at the Ames Laboratory. The Ames Laboratory is operated for the US Department of Energy by Iowa State University under Contract No. DE-AC02-07CH11358. In preparation for this work, RS did an undergraduate summer REU with DDJ at Illinois supported partially by the National Science Foundation (Grant No. DMR-07-05089).

APPENDIX A: DERIVATION OF THE NECESSARY CONDITIONS

We outline the derivation of Eq. (8), i.e., $w_{\rm APB} \leqslant 5.9a$. We also provide computed lattice constants, elastic constants, and APB and SF planar defect energies used for the necessary and sufficient condition design maps, with experimental values shown for comparison wherever available. Figure 2 shows the unit cells used for the three planar defect calculations.

First, recall that the self-energies of a screw and an edge dislocation are[66]

$$E_s = \frac{Gb_s^2}{4\pi}\ln\frac{r}{r_0}, \tag{A1}$$

$$E_e = \frac{Gb_e^2}{4\pi(1-\nu)}\ln\frac{r}{r_0}, \tag{A2}$$

where $G = c_{44}$ is the shear modulus; b_s and b_e are the Burgers vectors of the screw and edge dislocations, respectively; r_0 is the radius of the dislocation core; and r is the cutoff radius of the dislocation interaction. Note that r is finite because its strain field is canceled by the strain field of other dislocations.[67] The pure screw-screw and edge-edge interaction energies are[66]

$$E_{ss} = \frac{Gb_s^2}{2\pi}\ln\frac{r}{w}, \tag{A3}$$

$$E_{ee} = \frac{Gb_e^2}{2\pi(1-\nu)}\ln\frac{r}{w}, \tag{A4}$$

where w is the separation distance between APBs or SFs.

In Eq. (7a) of the main text, the $\langle 111\rangle$ screw dislocation dissociates into perfect dislocations along the cube edges; hence, there are no APBs or SFs. The dissociation does not result in any change in the total energy. Thus, with $\mathbf{b}_{a,s} = a\langle 111\rangle$ and $b_{a,s}^2 = 3a^2$, the total energy of the screw dislocation is

$$E_a = \frac{Gb_{a,s}^2}{4\pi}\ln\frac{r}{r_0} = \frac{3Ga^2}{4\pi}\ln\frac{r}{r_0}. \tag{A5}$$

In Eq. (7c) of the main text, the $\langle 111\rangle$ screw dislocation can dissociate into two $\frac{1}{2}\langle 111\rangle$ partials bounding an APB. The partials are purely screw, with Burgers vector $\mathbf{b}_{c,s} = \frac{a}{2}\langle 111\rangle$ and $b_{c,s}^2 = 3a^2/4$. Given the separation width $w_{\rm APB}$ of the partials, with planar defect energy $\gamma_{\rm APB}$, the total energy is

$$E_c = 2E_{c,s} + E_{c,ss} + \gamma_{\rm APB} w_{\rm APB}. \tag{A6}$$

We minimize the energy with respect to $w_{\rm APB}$, from which we find that

$$w_{\rm APB} = \frac{Gb_{c,s}^2}{4\pi\gamma_{\rm APB}} = \frac{3Ga^2}{8\pi\gamma_{\rm APB}}. \tag{A7}$$

Then, purely on energy grounds, in order for $\langle 001\rangle\{1\bar{1}0\}$ slip to be more favorable than APB$\{1\bar{1}0\}$ formation, E_a in Eq. (A5) must be less than E_c in Eq. (A6):

$$\frac{3Ga^2}{4\pi}\ln\frac{r}{r_0} < \frac{3Ga^2}{8\pi}\left(\ln\frac{r}{r_0} + \ln\frac{r}{w_{\rm APB}} + 1\right) \quad \text{or}$$

$$\ln\frac{w_{\rm APB}}{r_0} < 1. \tag{A8}$$

The dislocation core is $r_0 = ka$ for some constant k. Then, by Eq. (A8), the condition for $\langle 001\rangle$ slip is

$$\frac{w_{\rm APB}^{1\bar{1}0}}{a} < ke, \tag{A9}$$

or, in terms of the planar defect energy, as

$$\frac{\gamma_{\rm APB}^{1\bar{1}0}}{Ga} > \frac{3}{8\pi ke}, \quad \text{or} \tag{A10a}$$

$$\ln C > \ln\left(\frac{3}{8\pi ke}\right) \sim -3.126 - \ln k. \tag{A10b}$$

The core of the dislocation can be simulated using semiempirical and first-principles calculations, from which the radius of the core, and hence k, can be obtained for each B2 material. In general, r_0 has a range[68] of b to $5b$, so k is between $\sqrt{3}/2$ and $5\sqrt{3}/2$ in our case. Eshelby[69] estimated analytically r_0 to be about $1.5b$ for screw dislocations, which, according to Read,[70] is an underestimate. A simulation study by Xu and Moriarty[71] shows that $2b$, where $\mathbf{b} = \frac{a}{2}\langle 111\rangle$, is a good approximation for r_0 in bcc Mo. We expect the core radius to be somewhat larger in B2 systems than in bcc metals, since $\mathbf{b}$ represents a partial dislocation in B2 instead of a perfect

dislocation in bcc. Thus, we simply take r_0 to be between $2.5b$ ($k \approx 2.17$) and $5b$ ($k \approx 4.33$) for all B2 materials. Then ke in Eq. (A9) is between 5.9 and 11.8, which justifies the criterion imposed by Rachinger and Cottrell. For $k = 2.17$, we obtained Eq. (8), which gives the vertical line analytically in Fig. 3 at $\ln C = -3.9$ and provides a quantitative measure for comparison of many systems.

The derivation of the necessary [Eq. (9)] condition, $\delta > 0.119C^{-1/4}$, is more involved. It results from an energy-based comparison between APB and SF planar defect energies.[45] Equation (7b) shows that the $a\langle 001\rangle$ dislocation can further dissociate into $\frac{a}{2}\langle 001\rangle$ partial dislocations, creating a super-intrinsic stacking fault. The screw and edge components of the partial dislocation can be found by projecting $\frac{a}{2}\langle 001\rangle$ onto $a\langle 111\rangle$:

$$\frac{a}{2}\langle 001\rangle = \underbrace{\frac{a}{6}\langle 111\rangle}_{\mathbf{b}_{b,s}} + \underbrace{\frac{a}{6}\langle \bar{1}\bar{1}2\rangle}_{\mathbf{b}_{b,e}}. \tag{A11}$$

Thus, with $b_{b,s}^2 = a^2/12$ and $b_{b,e}^2 = a^2/6$, and using the self-energies from Eqs. (A1) and (A2) and the interaction energies from Eqs. (A3) and (A4), the total energy associated with SF formation is

$$E_b = \frac{Ga^2}{24\pi}\left(\ln\frac{r}{r_0} + \ln\frac{r}{w_{\mathrm{SF}}}\right) + \frac{Ga^2}{12\pi(1-\nu)}\left(\ln\frac{r}{r_0} + \ln\frac{r}{w_{\mathrm{SF}}}\right) + \gamma_{\mathrm{SF}} w_{\mathrm{SF}}. \tag{A12}$$

Minimizing energy with respect to w_{SF}, the separation width is found to be

$$w_{\mathrm{SF}} = \frac{3-\nu}{1-\nu}\frac{Ga^2}{24\pi\gamma_{\mathrm{SF}}}. \tag{A13}$$

Then Eq. (A12) becomes, with $\nu = 1/3$,

$$E_b = \frac{3-\nu}{1-\nu}\frac{Ga^2}{24\pi}\left(\ln\frac{r}{r_0} + \ln\frac{r}{w_{\mathrm{SF}}} + 1\right). \tag{A14}$$

Finally, we compare SF formation [Eq. (7b)] with APB formation [Eq. (7c)]. Note, we must multiply E_b by 3 for a fair comparison, since each $\langle 111\rangle$ dislocation dissociates into three families of $\langle 001\rangle$ dislocations, where each of them can create SFs independently. So, for APBs to be more energetically favorable than SFs, we need E_c in Eq. (A6) to be less than $3E_b$ in Eq. (A14); i.e.,

$$3\ln\frac{r}{w_{\mathrm{APB}}} - \frac{2\nu}{1-\nu}\left(1 + \ln\frac{r}{r_0}\right) < \frac{3-\nu}{1-\nu}\ln\frac{r}{w_{\mathrm{SF}}}. \tag{A15}$$

With $r_0 = ka$, and assuming consistently that $\nu = 1/3$ and $r = 2r_0 \approx 4.33a$, we get a criterion for APB formation to be more favorable than SF formation, i.e., Eq. (9).

APPENDIX B: ELASTIC CONSTANTS FOR BISTABILITY MAP

Here we provide an overview of how compliance elements S_{ij} are related to standard elastic constants c_{ij}. The derivations can be found by combining information in Refs. 46 and 47.

Bistability is determined by the anisotropic elastic response of the B2 lattice. M is a function of c_{ij}.[46,47] Let $H = 2c_{44} + c_{12} - c_{11} = (c_{11} - c_{12})(A - 1)$, where A is the Zener ratio, Eq. (1). Rotating the cubic elastic constants to the [111] axis yields

$$c'_{ij} = \begin{bmatrix} c'_{11} & c'_{12} & c'_{13} & 0 & c'_{15} & 0 \\ c'_{12} & c'_{11} & c'_{13} & 0 & -c'_{15} & 0 \\ c'_{13} & c'_{13} & c'_{33} & 0 & 0 & 0 \\ 0 & 0 & 0 & c'_{44} & 0 & -c'_{15} \\ c'_{15} & -c'_{15} & 0 & 0 & c'_{44} & 0 \\ 0 & 0 & 0 & -c'_{15} & 0 & c'_{66} \end{bmatrix}, \tag{B1}$$

where

$$c'_{11} = c_{11} + \frac{1}{2}H, \quad c'_{12} = c_{12} - \frac{1}{6}H,$$
$$c'_{13} = c_{12} - \frac{1}{3}H, \quad c'_{33} = c_{11} + \frac{2}{3}H,$$
$$c'_{44} = c_{44} - \frac{1}{3}H, \quad c'_{66} = c_{44} - \frac{1}{6}H,$$
$$c'_{15} = -\frac{\sqrt{2}}{6}H.$$

Note, for an isotropic material, $A = 1$, $H = 0$, and $c'_{ij} = c_{ij}$. The third row and column are deleted to obtain the inverse,[46] yielding

$$S_{ij} = \begin{bmatrix} S_{11} & S_{12} & 0 & S_{15} & 0 \\ S_{12} & S_{11} & 0 & -S_{15} & 0 \\ 0 & 0 & S_{44} & 0 & -2S_{15} \\ S_{15} & -S_{15} & 0 & S_{44} & 0 \\ 0 & 0 & -2S_{15} & 0 & S_{66} \end{bmatrix}, \tag{B2}$$

where

$$S_{11} = \frac{c'_{11}c'_{44} - c'^2_{15}}{2(c'_{11} + c'_{12})\left(c'_{44}c'_{66} - c'^2_{15}\right)},$$
$$S_{12} = -\frac{c'_{12}c'_{44} + c'^2_{15}}{2(c'_{11} + c'_{12})\left(c'_{44}c'_{66} - c'^2_{15}\right)},$$
$$S_{44} = \frac{c'_{66}}{c'_{44}c'_{66} - c'^2_{15}}, \quad S_{66} = \frac{c'_{44}}{c'_{44}c'_{66} - c'^2_{15}},$$
$$S_{15} = -\frac{c'_{15}}{2\left(c'_{44}c'_{66} - c'^2_{15}\right)}.$$

Finally, the parameter M is defined as

$$M = \sqrt{\frac{S_{11}S_{44}}{S_{11}S_{44} - S_{15}^2}}. \tag{B3}$$

As discussed by Sun,[48] $M \geqslant 1$, where the equality holds only for isotropic materials, where $A = 0$ and, hence, $H = 0$.

*ddj@AmesLab.gov

[1] K. Gschneidner, Jr., A. Russell, A. Pecharsky, J. Morris, Z. Zhang, T. Lograsso, D. Hsu, C. H. C. Lo, Y. Ye, A. Slager, and D. Kesse, Nat. Mater. **2**, 587 (2003).

[2] K. Gschneidner, Jr., M. Ji, C. Wang, K. Ho, A. Russell, Y. Mudryk, A. Becker, and J. Larson, Acta Mater. **57**, 5876 (2009).

[3] A. M. Russell, Adv. Eng. Mater. **5**, 629 (2003).

[4] A. M. Russell, Z. Zhang, K. A. Gschneidner, Jr., T. A. Lograsso, A. O. Pecharsky, A. J. Slager, and D. C. Kesse, Intermetallics **13**, 565 (2005).

[5] K. Gschneidner, Jr. (private communication).

[6] M. Yamaguchi and Y. Umakoshi, Prog. Mater. Sci. **34**, 1 (1990).

[7] I. Baker, Mater. Sci. Eng. A **192**, 1 (1995).

[8] A. M. Russell, Z. Zhang, T. A. Lograsso, C. C. H. Lo, A. O. Pecharsky, J. R. Morris, Y. Ye, K. A. Gschneidner, Jr., and A. J. Slager, Acta Mater. **52**, 4033 (2004).

[9] G. H. Cao, D. Shechtman, D. M. Wu, A. T. Becker, L. S. Chumbley, T. A. Lograsso, A. M. Russell, and K. A. Gschneidner, Jr., Acta Mater. **55**, 3765 (2007).

[10] J. R. Morris, Y. Ye, Y. B. Lee, B. N. Harmon, and K. Gschneidner, Jr., Acta Mater. **52**, 4849 (2004).

[11] Q. Chen and S. B. Biner, Acta Mater. **53**, 3215 (2005).

[12] J. R. Morris, Y. Ye, M. Krcmar, and C. L. Fu, Mater. Res. Soc. Symp. Proc. **980**, 113 (2007).

[13] J. B. Liu, D. D. Johnson, and A. V. Smirnov, Acta Mater. **53**, 3601 (2005).

[14] V. Paidar, D. P. Pope, and M. Yamaguchi, Scr. Metall. **15**, 1029 (1981).

[15] G. Saada and P. Veyssiere, Philos. Mag. A **66**, 1081 (1992).

[16] P. Hohenberg and W. Kohn, Phys. Rev. **136**, B864 (1964).

[17] W. Kohn and L. J. Sham, Phys. Rev. **140**, A1133 (1965).

[18] G. Kresse and J. Hafner, Phys. Rev. B **47**, 558 (1993).

[19] G. Kresse and J. Hafner, Phys. Rev. B **49**, 14251 (1994).

[20] G. Kresse and J. Furthmüller, Phys. Rev. B **54**, 11169 (1996).

[21] G. Kresse and J. Furthmüller, Comput. Mater. Sci. **6**, 15 (1996).

[22] P. E. Blöchl, Phys. Rev. B **50**, 17953 (1994).

[23] G. Kresse and D. Joubert, Phys. Rev. B **59**, 1758 (1999).

[24] J. P. Perdew and A. Zunger, Phys. Rev. B **23**, 5048 (1981).

[25] J. P. Perdew and Y. Wang, Phys. Rev. B **45**, 13244 (1992).

[26] H. J. Monkhorst and J. D. Pack, Phys. Rev. B **13**, 5188 (1976).

[27] D. D. J. S. Kibey, J. B. Liu, and H. Sehitoglu, Acta Mater. **55**, 6843 (2007).

[28] S. A. Kibey, L. L. Wang, J. B. Liu, H. T. Johnson, H. Sehitoglu, and D. D. Johnson, Phys. Rev. B **79**, 214202 (2009).

[29] M. J. Mehl, B. M. Klein, and D. A. Papaconstantopolous, in *Intermetallic Compounds: Principles and Practice*, edited by J. H. Westbrook and R. L. Fleischer (Wiley, London, 1995), Chap. 9, p. 195.

[30] D. Seipler, B. Bremicker, U. Goebel, H. Happel, H. E. Hoenig, and B. Perrin, J. Phys. F **7**, 599 (1977).

[31] D. G. Nagengast, A. T. M. van Gogh, E. S. Kooij, B. Dam, and R. Griessen, Appl. Phys. Lett. **75**, 2050 (1999).

[32] C. C. Chao, H. L. Luo, and P. Duwez, J. Appl. Phys. **35**, 257 (1964).

[33] J. Kübler, J. Phys. F **8**, 2301 (1978).

[34] A. Palenzona and P. Manfrinetti, J. Alloys Compd. **257**, 224 (1997).

[35] N. Arıkan and Ş. Uğur, Comput. Mater. Sci. **47**, 668 (2010).

[36] T. H. Geballe, B. T. Matthias, V. B. Compton, E. Corenzwit, G. W. Hull, and L. D. Longinotti, Phys. Rev. **137**, A119 (1965).

[37] W. B. Pearson, *A Handbook of Lattice Spacings and Structures of Metals and Alloys*, Vol. 2 (Pergamon, Oxford, 1967).

[38] G. Simmons and H. Wang, *Single Crystal Elastic Constants and Calculated Aggregate Properties: A Handbook*, 2nd ed. (MIT Press, Cambridge, MA, 1971).

[39] G. Saada and P. Veyssiere, Phys. Status Solidi B **172**, 309 (1992).

[40] R. J. Schiltz, Jr., T. S. Prevender, and J. F. Smith, J. Appl. Phys. **42**, 4680 (1971).

[41] D. Lazarus, Phys. Rev. **76**, 545 (1949).

[42] S. Satpathy, Phys. Rev. B **33**, 8706 (1986).

[43] A. Smakula and J. Kalnajs, Phys. Rev. **99**, 1737 (1955).

[44] W. A. Rachinger and A. H. Cottrell, Acta Metall. **4**, 109 (1956).

[45] R. Sun, Senior thesis, University of Illinois at Urbana-Champaign (2008), http://hdl.handle.net/2142/42599.

[46] A. K. Head, Phys. Status Solidi **6**, 461 (1964).

[47] J. P. Hirth and J. Lothe, *Theory of Dislocations* (Krieger, Malabar, FL, 1992).

[48] Y. Q. Sun, Acta Metall. Mater. **43**, 3775 (1995).

[49] A. Ball and R. E. Smallman, Acta Metall. **14**, 1517 (1966).

[50] M. Yamaguchi and Y. Umakoshi, Acta Metall. **24**, 1061 (1976).

[51] D. Wu, I. Baker, P. R. Munroe, and E. P. George, Intermetallics **15**, 103 (2007).

[52] T. Yamagata and H. Yoshida, Mater. Sci. Eng. **12**, 95 (1973).

[53] T. Yamagata, J. Phys. Soc. Jpn. **45**, 1575 (1978).

[54] H. Häkkinen, M. Moseler, and U. Landman, Phys. Rev. Lett. **89**, 033401 (2002).

[55] J. R. Morris and Y. Y. Ye (private communication).

[56] C. L. Fu and M. H. Yoo, Acta Metall. Mater. **40**, 703 (1992).

[57] H. Saka, M. Kawase, A. Nohara, and T. Imura, Philos. Mag. A **50**, 65 (1984).

[58] G. Dirras, P. Beauchamp, and P. Veyssiere, Philos. Mag. A **65**, 815 (1992).

[59] J. Brown, R. Srinivasan, M. J. Mills, and M. S. Daw, Philos. Mag. A **80**, 2855 (2000).

[60] J. Moriarty, J. Humphreys, R. Gordon, and N. Baenziger, Acta Crystallogr. **21**, 840 (1966).

[61] S. Yatsenko, A. Semyannikov, H. Shakarov, and E. Fedorova, J. Less-Common Met. **90**, 95 (1983).

[62] K. Gschneidner, Jr., Y. Mudryk, A. Becker, and J. Larson, CALPHAD: Comput. Coupling Phase Diagrams Thermochem. **33**, 8 (2009).

[63] S. Ogata, J. Li, and S. Yip, Science **298**, 807 (2002).

[64] V. Paidar, Yi-Shen Lin, M. Cak, and V. Vitek, Intermetallics **18**, 1285 (2010).

[65] R. Schroll, V. Vitek, and P. Gumbsch, Acta Mater. **46**, 903 (1998).

[66] F. R. N. Nabarro, Adv. Phys. **1**, 269 (1952).

[67] T. H. Courtney, *Mechanical Behavior of Materials*, 2nd ed. (McGraw-Hill, Boston, MA, 2000).

[68] D. Hull and D. J. Bacon, *Introduction to Dislocations*, 4th ed. (Butterworth-Heinemann, Woburn, MA, 2001).

[69] J. D. Eshelby, Proc. Phys. Soc. A **62**, 307 (1949).

[70] W. T. Read, *Dislocations in Crystals* (McGraw-Hill, New York, 1953).

[71] W. Xu and J. A. Moriarty, Phys. Rev. B **54**, 6941 (1996).